

Analysis for Effective Flange Width Considering Slip Effect for Main Girder of Composite Cable stayed Bridges during Construction Phase

Hua Luo, Jianqiang Feng, Qincong She, Bin Li, Changqing Wu, Mingdeng Pan and Yongqing Zeng,
Member, IAENG

Abstract—In composite girder cable-stayed bridges, the concrete deck slab experiences pronounced warping deformation due to the combined effects of bending moments and axial forces, leading to an uneven distribution of stress across its cross-section. To resolve this structural challenge, engineering practitioners adopt the effective flange width principle to account for shear lag effects in composite section design, as stipulated in structural design codes. However, the presence of anchored cables leads to a non-uniform distribution of the effective width along the span, an issue that has received limited research attention to date. This study aims to fill this gap by developing a nonlinear finite element (FE) model using ABAQUS, which is subsequently validated through in situ measurements from the Chibi Yangtze River Bridge: the world's largest steel-concrete composite girder cable-stayed bridge, features a main span of 720 meters. The FE model demonstrated its capability to accurately predict the behavior of such girders, thereby enabling a more precise calculation of the effective slab width. Based on the envelope diagram illustrating the longitudinal distribution of the effective width for the main girder during critical construction phases of the Chibi Yangtze River Bridge, this study proposes a calculation method for determining the effective width of the concrete deck slab under the influence of self-weight and cable tension. The findings reveal that under the axial pressure exerted by the cables, the effective width of the deck slab exhibits localized oscillations along the bridge's longitudinal axis. Specifically, the

effective width coefficient in these oscillating regions follows a pattern where it is greatest at the cable anchorage section, followed by the section connected to the crossbeam, and smallest at the intermediate section between two cables. The proposed method for calculating the effective width comprehensively accounts for significant variations in the deck slab's effective width near the main tower bearings, auxiliary piers, beam ends, and the mid-span of the main span. By integrating finite element analysis (FEA) with construction site validations, this research establishes robust tools for engineering design, contributing to the construction of safe and serviceable cable-stayed bridges. Furthermore, this study enhances the understanding of shear lag behavior and emphasizes the importance of appropriately considering its effects in bridge analysis and design. The comprehensive investigation significantly advances the knowledge of effective flange width in composite girders of cable-stayed bridges, providing a solid foundation for future research and practical applications.

Index Terms—cable-stayed bridge, steel concrete composite girder, construction phase, slippage, effective flange width

I. INTRODUCTION

STEEL concrete composite structural systems, integrating principles of prefabricated assembly, sustainable construction practices, low-carbon material optimization, life-cycle maintainability, and intelligent design integration, have emerged as a preferred solution for long-span bridge engineering applications, particularly in cable-stayed bridge configurations. In such configurations, stay cables induce localized compressive stresses through welded anchorage assemblies on the steel girder's upper flange, creating transverse normal stress gradients across the composite deck cross-section [1,2]. Neglecting this shear lag phenomenon may lead to 15-20% underestimation of critical deformations and peak stresses under serviceability limit states, potentially initiating premature concrete cracking. Current design practice adopts the effective flange width principle, which idealizes the concrete slab's effective width as participating fully with the steel girder in longitudinal bending resistance through calibrated reduction coefficients. This analytical simplification assumes uniform stress distribution in the concrete flange, necessitating precise determination of effective width parameters to ensure accurate predictions of composite stiffness and ultimate bearing capacity.

To evaluate the effective width of composite girders, various researchers have introduced innovative methodologies. Notably, Nicoletti [3] developed 120 finite

Manuscript received January 14, 2025; revised March 30, 2025.

This work was supported by the Program of Hunan Province Education Department (Grant Nos. 23A0496, 22A0472 and 23B0645), the Teaching Reform Research Project of Hunan Institute of Science and Technology (Grant No. 2024A02), the Hunan Province Degree and Graduate Education Reform Research Project (Grant No. 2024JGZD060), and the Innovation Project of Hunan Undergraduate Students, China (Grant No. S202412658014).

Hua Luo is an associate professor of Civil Engineering and Architecture, Hunan Institute of Science and Technology, Yueyang, 414000, China (e-mail: 12015024@hnist.edu.cn).

Jianqiang Feng is a postgraduate student in College of Civil Engineering and Architecture, Hunan Institute of Science and Technology, Yueyang, 414000, China (e-mail: 82221140531@vip.hnist.edu.cn).

Qincong She is a lecturer in College of Civil Engineering and Architecture, Hunan Institute of Science and Technology, Yueyang, 414000, China (corresponding author to provide e-mail: 22017036@hnist.edu.cn).

Bin Li is an associate professor in College of Civil Engineering and Architecture, Hunan Institute of Science and Technology, Yueyang, 414000, China (e-mail: 12007030@hnist.edu.cn).

Mingdeng Pan is an undergraduate student in College of Civil Engineering and Architecture, Hunan Institute of Science and Technology, Yueyang, 414000, China (e-mail: 2590244010@qq.com).

Changqing Wu is a lecturer in College of Civil Engineering and Architecture, Hunan Institute of Science and Technology, Yueyang, 414000, China (e-mail: 12021048@hnist.edu.cn).

Yongqing Zeng is an associate professor in College of Civil Engineering and Architecture, Hunan Institute of Science and Technology, Yueyang 414000, China (e-mail: 1013433575@qq.com).

element models to investigate the influence of several factors, including the degree of steel-concrete interaction, section configuration, height of the concrete top slab, and span length, on the effective width of steel-concrete composite box girders. The findings revealed a linear relationship between the effective width and both the thickness of the concrete slab and the span length. Additionally, Nicoletti proposed a standardized method for calculating the effective width correction coefficient for partially connected steel-concrete composite girders. Yuan [4] investigated the variation patterns of the shear lag effect during the construction process of a cable-stayed bridge featuring corrugated steel webs by examining three representative control sections. The study revealed that as the cantilever length increased, the shear lag coefficients for both the top and bottom slabs exhibited a gradual upward trend. In addition, a significant reduction in the shear lag coefficient was observed following the closure of the bridge. Furthermore, the analysis demonstrated that the shear lag effect reached its maximum intensity in the vicinity of the main tower section. Jiang [5] investigated the factors influencing the effective flange width in the negative moment region of externally inverted U-shaped steel-concrete simply supported composite beams through experimental research on bending performance in the negative moment area. The study comprehensively analyzed the effects of load type, width-span ratio, and thickness ratio on the effective flange width in both elastic and elastoplastic stages for the mid-span section. The findings demonstrate that the effective flange width under uniformly distributed load exceeds that under non-uniformly distributed load across different load types, while the influence of thickness ratio on the effective flange width is negligible. Chen [6] developed a finite element model based on the G1503 highway bridge spanning the Wusong River, focusing on a composite continuous steel box girder bridge configuration. The study investigated the variation patterns of the effective width coefficient in the composite bridge deck of long-span closed steel box girders. The analysis revealed two significant findings: (1) the transverse stress distribution patterns between the steel deck slab and concrete deck slab exhibit remarkable similarity; (2) the effective width of the steel slab demonstrates close alignment with standard specification requirements. Lin [7] developed a finite element model to analyze the effective width coefficient of concrete in the composite beam section, using a high-speed railway cable-stayed bridge as a case study, with particular focus on both the mid-span and tower regions. The analysis reveals two distinct trends: (1) under cable-induced axial compression, the concrete's effective width coefficient exhibits a progressive increase from the mid-span toward the bridge tower; (2) conversely, under bending moment, the coefficient demonstrates a gradual decrease from the mid-span to the tower. Wen [8] developed spatial finite element models for three-span composite continuous girders with variable stiffness, investigating the effects of two key factors: (1) the construction of the bottom concrete slab in the variable stiffness region, and (2) the shear stiffness at the

steel-concrete interface. The study focused on their influence on both the effective width and longitudinal stress distribution of the top concrete slab. The analysis demonstrates a strong correlation between the effective width calculations for the top concrete slab—specifically at the mid-span section of the side span and the support section of the mid-span—obtained through finite element analysis and those derived from British and Japanese standards, with discrepancies consistently maintained below 15%. Zhou [9] conducted a comprehensive investigation combining experimental studies and spatial finite element analysis to determine stress values in the segmental girder model under two loading conditions: prestressing cable tension and service load. The research findings suggest that the effective flange width calculation for the separated double main rib section under axial force can be accurately performed using a 26.18° angle distribution assumption. Nie [10] performed a comprehensive spatial finite element analysis focusing on the concrete deck of a composite girder and its stress transmission characteristics under axial force, utilizing data from an actual long-span composite cable-stayed bridge project. The analysis reveals that axial force-induced stresses in the concrete deck propagate linearly along the main girder's sides at a 27° angle. Furthermore, while the stress distribution pattern is influenced by crossbeam spacing, this effect is negligible in practical applications. Zhai [11] conducted a comprehensive finite element analysis to investigate the distribution characteristics of the effective flange width coefficient along the span under combined axial and bending forces. The analysis identified 28° as the optimal stress transmission angle for axial forces induced by stay cable compression. Furthermore, the proposed practical calculation method for determining the effective slab width coefficient in long-span composite cable-stayed bridges under combined axial and bending actions accurately captures the stress distribution in the concrete deck plate. Gian [12] developed an innovative methodology for evaluating stress distribution and structural resistance in composite decks, accounting for the combined effects of axial forces and bending moments in cable-supported structures. This comprehensive approach addresses both serviceability limit states and ultimate limit states, providing a robust framework for structural assessment. Zhang [13] developed a novel methodology for calculating the shear lag coefficient in twin I-shaped composite girders (TICGs) of cable-stayed bridges, utilizing the principle of additional deflection. This innovative approach provides a more accurate assessment of shear lag effects in such structural configurations. Wen [14] conducted comprehensive experimental and finite element (FE) investigations to examine the effective width characteristics of both single and twin I-beam composite girders. The research employed an extensive set of sixty-nine FE models to systematically analyze the influence of key parameters, including slab thickness, web configuration, shear stud interaction degree (ID), and width-to-span ratio, as well as their interdependent effects on the effective width. Huang [15] developed an

advanced simulation-based methodology for simultaneously predicting both the effective flange width and ultimate load capacity in steel-concrete composite beams incorporating transverse and longitudinal hidden girders. Silva [16] conducted a comprehensive investigation into the structural behavior of steel-concrete composite box girder bridges under partial interaction conditions. The study systematically evaluated the influence of three key parameters: (1) slab height, (2) longitudinal span length, and (3) cross-sectional configuration, on the effective width characteristics of the composite system. Zhu [17] developed an advanced analytical model utilizing Gene Expression Programming (GEP) to accurately determine the load-effective distribution width of deck slabs in steel-concrete composite box girders. This innovative approach provides a comprehensive computational framework that is applicable across both elastic and elastoplastic stages of structural behavior. Mahmoud [18] conducted an extensive numerical investigation to develop novel predictive equations for determining effective concrete slab width across varying loading conditions. The study revealed that the effective width is primarily governed by two key dimensionless parameters: (1) the slenderness ratio (L/r_s) of the steel beam and (2) the slab width-to-span ratio (B_s/L). Laura [19] conducted a comprehensive investigation into the structural behavior of steel-concrete composite beams, with particular emphasis on effective slab width determination under nonlinear shear connection conditions. The research systematically examined the influence of partial interaction effects on the effective width characteristics of concrete slabs in composite beam systems. This study incorporated the critical consideration of load-dependent shear stiffness variations attributable to interfacial slip phenomena.

Extensive research has revealed significant variations in effective width values between structures subjected to pure axial compression and those under pure bending moments. When considering the combined action of axial forces and bending moments during construction stages, these effective width values diverge substantially from those observed under single loading conditions. Notably, empirical studies demonstrate that under normal service conditions, the concrete deck slab can bear over 75% of the total axial force. However, current research predominantly assumes perfect shear connection between the steel main girder and concrete deck slab, neglecting potential interfacial slip, a critical limitation given that practical engineering applications inevitably experience some degree of slip at this interface. This oversight is particularly significant as slip effects can substantially influence stress distribution patterns within the deck slab, potentially leading to considerable inaccuracies in effective width calculations. Furthermore, current design standards provide specifications only for pure axial compression or bending scenarios, lacking comprehensive guidelines for determining effective width coefficients in composite cable-stayed bridges under combined compression-bending actions. The absence of specific regulatory guidelines, combined with the significant impact

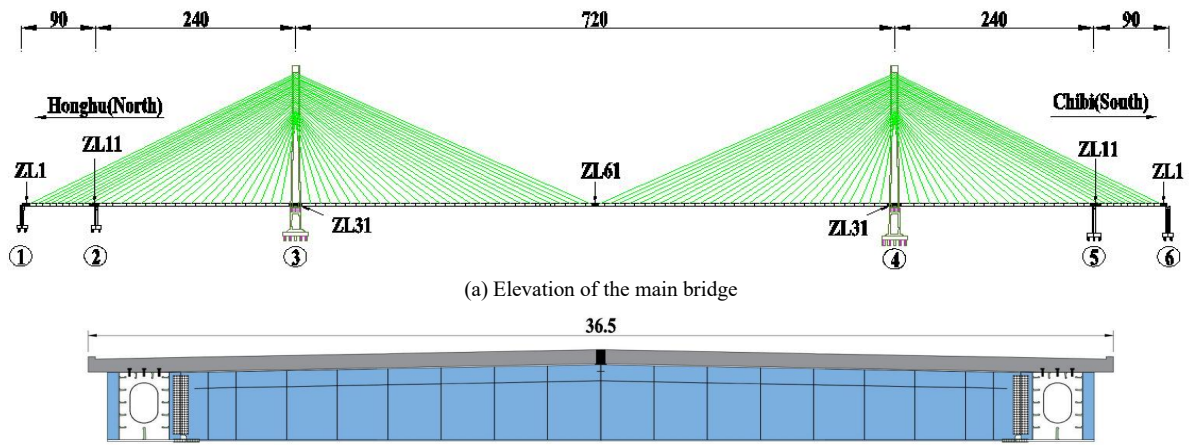
of slip effects, highlights the critical need for comprehensive research into effective width characteristics in twin box-shaped composite girders of cable-stayed bridges. This investigation is particularly crucial during the construction phase, where complex combined loading conditions are most frequently encountered.

The subsequent sections of this paper are structured as follows. Section 2 presents a comprehensive description of the Chibi Yangtze River Bridge project, accompanied by detailed analysis of in-situ testing results. Section 3 describes the development and validation of a finite element (FE) analysis model specifically designed to simulate transverse stress distribution patterns under typical construction conditions, with model accuracy rigorously verified through field measurement comparisons. Section 4 proposes a novel framework for determining longitudinal distribution of slab effective width, providing critical insights for the longitudinal analysis and design of composite cable-stayed bridges. This research aims to establish a robust theoretical foundation that will enhance the design of steel-concrete composite structures in future engineering applications.

II. IN-SITU TESTING OF THE MAIN GIRDER OF A CABLE STAYED BRIDGE DURING CONSTRUCTION STAGE

A. Bridge Overview

The Chibi Yangtze River Bridge features a world-class steel-concrete composite girder cable-stayed bridge design with dual pylons and double cable planes, as illustrated in Fig. 1(a). With a remarkable span arrangement of (90+240+720+240+90) meters, the bridge boasts a 720-meter main span—currently the longest in its category worldwide. The bridge superstructure, measuring 36.5 meters in width, employs an innovative twin-box cross-section configuration, as depicted in Fig. 1(b). The main girder features a twin-box section configuration, comprising a steel box girder and a precast concrete deck. In a standard segment, the steel box girder has a depth of 3.181 meters, while the concrete deck measures 26 centimeters in thickness. These structural components are interconnected through shear connectors strategically positioned on the longitudinal beams, transverse beams, and auxiliary longitudinal beams. The standard segment's main steel girder, spanning 12 meters longitudinally and 35.12 meters transversely, comprises two side steel box girders complemented by three transverse steel beams (spaced at 4-meter intervals) and auxiliary longitudinal beams. The stay cable system is anchored to the main girder through specialized anchor plates positioned directly above the intersection of the central transverse beam and the outer web of the side box girder. The cable arrangement demonstrates variable spacing, with 12-meter intervals in the central span and 8, 12, or 16-meter spacing in the side spans, reflecting optimal load distribution considerations. The bridge's construction employed the balanced cantilever method, ensuring symmetrical progression from both ends. The steel girder system is longitudinally segmented into 121 sections, comprising 60 sections on each side (designated ZL1 to ZL60) and a central closure section (ZL61).



(a) Elevation of the main bridge
 (b) Standard cross-section of composite girder
 Fig. 1 The Chibi Yangtze River Bridge (units: m)

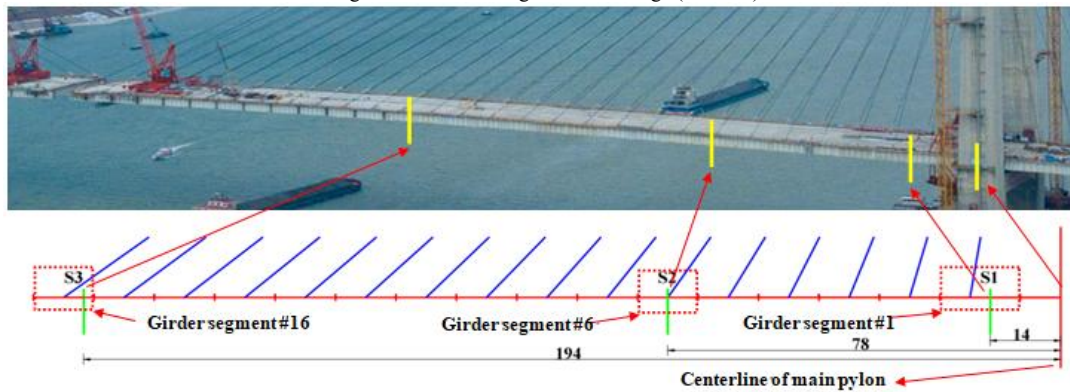


Fig. 2 Test girder segments and test sections (unit: mm)

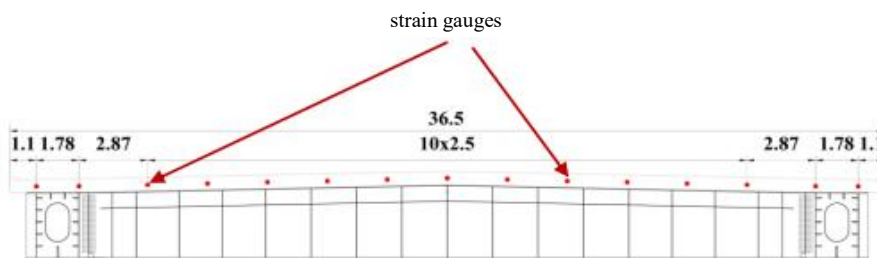
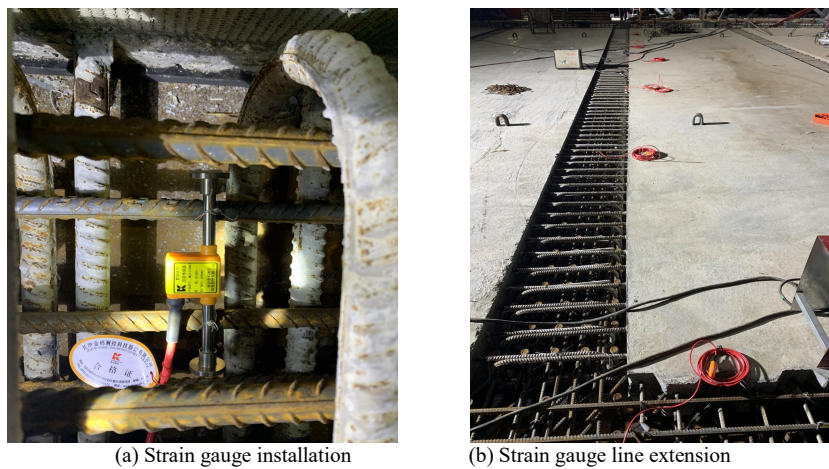


Fig. 3 Transverse arrangement of strain gauges on the test section (unit: m)



(a) Strain gauge installation
 (b) Strain gauge line extension
 Fig. 4 Field installation of strain gauges

B. Layout of measuring points on the main girder

In order to grasp the real-time stresses in the concrete deck

during the construction of the bridge's main girder, three concrete stress test sections (S1, S2, and S3) were established. Section S1 is located in girder segment #1, 14 meters from

the tower center-line; Section S2 is positioned in girder segment #6, 78 meters from the tower center-line; and Section S3 is situated in girder segment #16, 194 meters from the tower center-line, as illustrated in Fig. 2. Each section was equipped with a total of 15 strain gauges. The transverse arrangement of the strain gauges on the test sections is depicted in Fig. 3. Figure 4 shows the field installation of strain gauges.

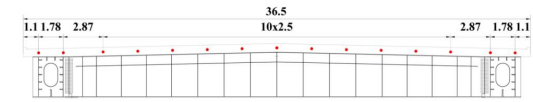
C. The field-measured stress on the concrete deck slab of the main girder during construction phase

The main span of the Chibi Yangtze River Highway Bridge was constructed symmetrically using the double cantilever segmental assembly method. Throughout the segmental construction process, the internal forces and stresses within the concrete bridge deck underwent continuous variations. Stress distributions along the longitudinal direction of the bridge deck were analyzed under six typical construction conditions (Table I), with detailed results presented in Table II, Table III, Table IV, and Figure 5. As illustrated in Figure 5, the stress distribution across the deck slab exhibited non-uniform characteristics in the transverse direction during the main girder construction, demonstrating a significant shear-lag effect. This shear-lag phenomenon became progressively more pronounced with the increasing number of cantilever segments. Under construction condition CC6, the following stress characteristics were observed: 1) At section S1, the analytical maximum stress at the top surface of the concrete slab reached -13.9 MPa, while the theoretical stress was -9.7 MPa, yielding a shear-lag coefficient of 1.433; 2) At section S2, the analytical maximum stress at the top surface measured -10.8 MPa, compared to the theoretical stress of -8.9 MPa, resulting in a shear-lag coefficient of 1.213; 3) At section S3, the analytical maximum stress at the top surface was -9.23 MPa, versus the theoretical stress of -6.4 MPa, producing a shear-lag coefficient of 1.442. Furthermore, a particularly notable stress concentration phenomenon was identified at the junction between the side box girders and small longitudinal beams. These findings underscore the importance of considering shear-lag effects during the construction phase of cable-stayed bridges.

TABLE I
SIX TYPICAL CONSTRUCTION CONDITIONS

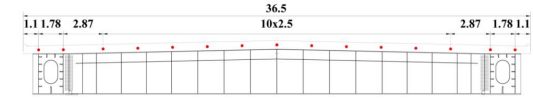
Working conditions	Description
Condition 1-CC1	Completion of two tensioning operations for girder segment #1 (CZ1/CB1)
Condition 2-CC2	Completion of two tensioning operations for girder segment #6 (CZ6/CB6)
Condition 3-CC3	Completion of two tensioning operations for girder segment #16 (CZ16/CB16)
Condition 4-CC4	Completion of two tensioning operations for girder segment #18 (CZ18/CB18)
Condition 5-CC5	Completion of two tensioning operations for girder segment #24 (CZ24/CB24)
Condition 6-CC6	Completion of two tensioning operations for girder segment #29 (CZ29/CB29) (Maximum balanced cantilever construction stage)

TABLE II
MEASURED VALUES OF STRESSES ON SECTION S1 (UNIT: MPA)



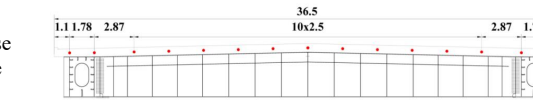
Transverse Distance /m	CC1	CC2	CC3	CC4	CC5	CC6
-17.15	-0.74	-2.30	-5.88	-6.90	-8.40	-13.90
-15.37	-0.50	-1.78	-5.74	-6.60	-7.35	-13.20
-12.5	-0.36	-1.46	-3.90	-4.00	-5.70	-8.60
-10	-0.27	-1.92	-3.29	-3.20	-6.61	-8.70
-7.5	-0.15	-1.41	-3.99	-3.80	-5.93	-7.70
-5	-0.20	-1.57	-3.30	-3.80	-5.84	-8.40
-2.5	-0.12	-1.43	-3.29	-4.20	-5.53	-9.20
0	-0.10	-1.33	-4.80	-5.30	-6.86	-10.20
2.5	-0.10	-1.43	-3.39	-3.60	-5.63	-7.80
5	-0.20	-1.57	-3.00	-3.60	-5.54	-9.80
7.5	-0.23	-1.41	-2.99	-4.30	-4.93	-7.80
10	-0.23	-1.92	-2.39	-3.60	-5.71	-8.70
12.5	-0.23	-1.46	-3.20	-4.20	-5.00	-7.70
15.37	-0.46	-1.78	-5.54	-6.30	-7.15	-13.50
17.15	-0.60	-2.30	-5.78	-6.50	-8.30	-12.80

TABLE III
MEASURED VALUES OF STRESSES ON SECTION S2 (UNIT: MPA)



Transverse Distance /m	CC2	CC3	CC4	CC5	CC6
-17.15	-0.36	-3.84	-5.20	-8.40	-10.80
-15.37	0.23	-3.23	-4.80	-7.64	-9.80
-12.5	-0.47	-4.61	-6.00	-6.58	-9.20
-10	-0.27	-4.40	-5.30	-6.32	-8.00
-7.5	-0.27	-4.38	-5.80	-6.21	-8.00
-5	-0.27	-3.63	-6.30	-5.44	-7.80
-2.5	-0.65	-4.74	-5.80	-6.63	-7.80
0	-0.08	-3.69	-4.20	-7.88	-9.60
2.5	-0.25	-3.90	-5.00	-6.10	-7.00
5	-0.07	-4.13	-6.80	-6.24	-8.60
7.5	-0.57	-4.08	-5.70	-6.21	-7.80
10	-0.27	-3.63	-6.20	-5.85	-7.90
12.5	-0.17	-2.99	-5.00	-5.25	-8.50
15.37	0.23	-3.06	-3.60	-7.77	-10.00
17.15	-0.16	-2.23	-4.80	-7.10	-8.84

TABLE IV
MEASURED VALUES OF STRESSES ON SECTION S3 (UNIT: MPA)



Transverse Distance /m	CC3	CC4	CC5	CC6
-17.15	-1.79	-2.70	-5.52	-9.23
-15.37	-0.82	-2.12	-4.29	-8.06
-12.5	-0.23	-0.90	-2.55	-5.57
-10	-0.09	-1.20	-2.54	-5.22
-7.5	-0.15	-1.12	-2.64	-5.43
-5	0.07	-1.30	-2.93	-5.42
-2.5	0.14	-1.44	-2.93	-5.15
0	-0.34	-1.80	-4.52	-7.06
2.5	-0.25	-1.05	-3.32	-5.79
5	-0.13	-1.10	-3.14	-5.96
7.5	0.02	-1.30	-2.46	-5.22
10	-0.09	-1.20	-2.54	-6.04
12.5	0.13	-1.27	-2.18	-6.21
15.37	-0.74	-2.20	-4.21	-7.95
17.15	-1.59	-2.90	-5.32	-8.84

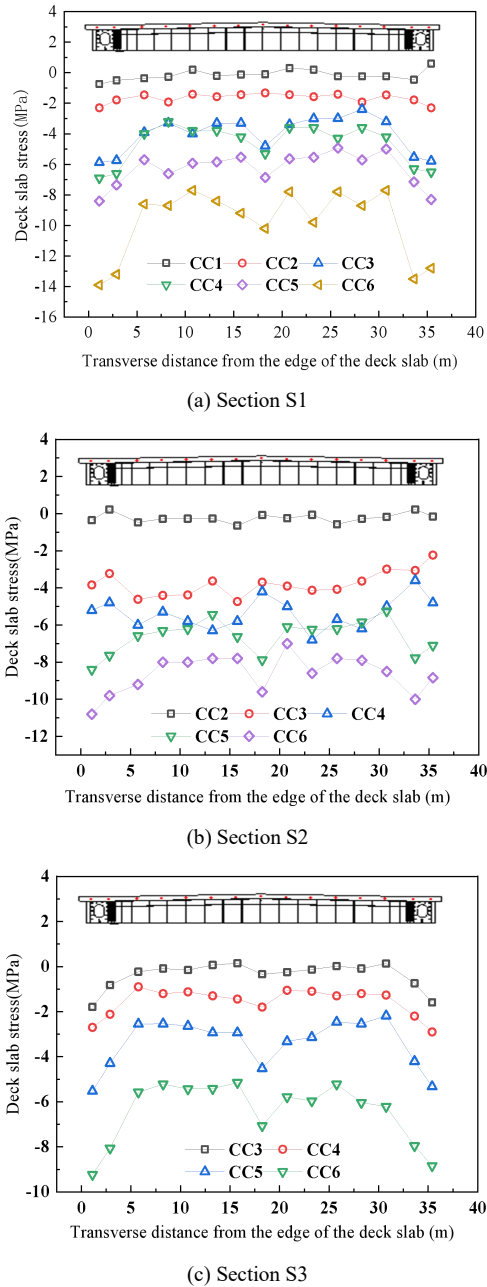


Fig. 5 Measured values of stresses on sections S1-S3

III. FINITE ELEMENT ANALYSIS

A. Global Modeling with Midas Civil

A comprehensive bridge analysis model was developed using beam elements in Midas Civil (Fig. 6). By monitoring the structural, boundary, and load variations at each construction stage, the global internal force distribution of the bridge across different construction phases was determined.

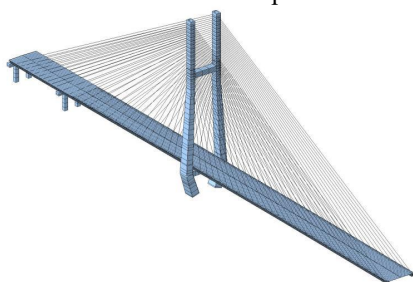
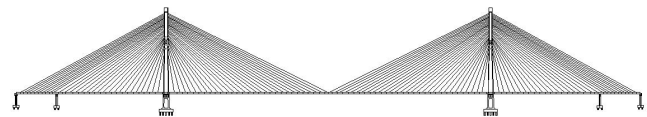


Fig. 6 Global beam element analysis model of the 1/2 Cable-Stayed Bridge (Maximum balanced cantilever construction stage)

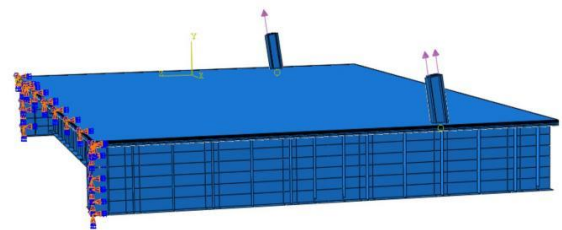
B. Local Modeling with ABAQUS

A detailed spatial local computational solid model (Fig. 7) for each construction stage of the Chibi Yangtze River Bridge was developed using ABAQUS. The concrete deck slab and anchor plates were modeled using three-dimensional eight-node solid elements with reduced integration (C3D8R). The main steel girder, which includes longitudinal beams, transverse beams, and small longitudinal beam, was represented using four-node shell elements with reduced integration (S4R). To ensure computational accuracy, nine Simpson's integration points were employed across the thickness of the shell elements. Furthermore, to simulate the slip effect between the steel main girder and the bridge deck, spring elements were utilized to model the connection behavior of the shear studs. This approach considered only the longitudinal slip direction while neglecting transverse displacements and any potential uplift of the concrete deck.

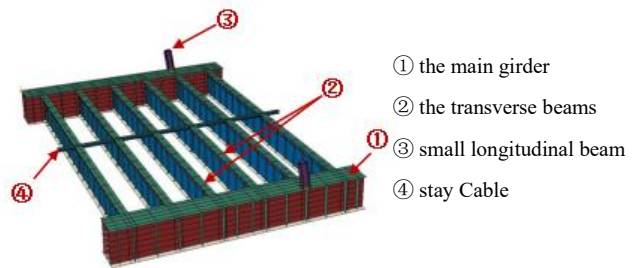
During the construction of the three segments at the top of the main girder and pier, temporary three-way fixation measures (in the longitudinal, transverse, and vertical directions) were implemented at the construction site to secure the connection between the main girder and the main tower. These measures were essential to ensure the structural stability and safety throughout the construction process. To accurately reflect the actual engineering conditions, the boundary conditions of the main girder in the tower area were modeled as fixed (Fig. 7(b)). The cable forces for the stay cables were derived from the overall bar system model (as illustrated in Fig. 7(a)), corresponding to the specific requirements of each construction stage.



(a) Overall model of the full bridge



(b) Local spatial FE model (Boundary conditions)



(c) Local spatial FE model (Connection detail between main girder and transverse beam)

Fig. 7 Finite Element Model

C. Experimental set-up and procedures

Using CC6 as a representative case, a comparative analysis was conducted among the field-measured data, ABAQUS

simulation results, and elementary beam theory values. The detailed comparative data are presented in Fig. 8.

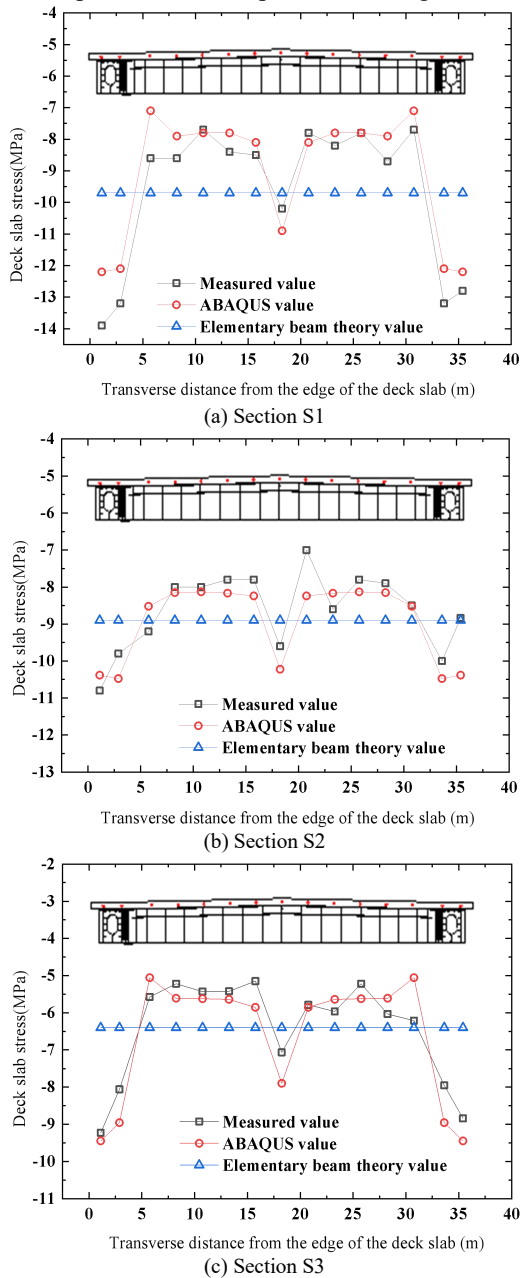


Fig. 8 Measured and calculated values of stresses on test sections (CC6)

As illustrated in Fig. 8, under working condition CC6, the following observations were made: 1) For Section S1, the maximum measured stress on the top surface of the concrete slab was -13.9 MPa, while the corresponding finite element analysis yielded -12.2 MPa, and the elementary beam theory calculation resulted in -9.7 MPa, with shear-lag coefficients of 1.433 and 1.258, respectively; 2) In Section S2, the maximum measured stress reached -10.8 MPa, compared to the finite element calculation of -10.38 MPa and the elementary beam theory value of -8.9 MPa, accompanied by shear-lag coefficients of 1.213 and 1.166; 3) Section S3 demonstrated a maximum measured stress of -9.23 MPa, with finite element and elementary beam theory calculations of -9.45 MPa and -6.4 MPa, respectively, and corresponding shear-lag coefficients of 1.442 and 1.477. The comparative analysis reveals that the maximum discrepancy between ABAQUS simulations and field-measured data is 12.23%, the transverse distribution patterns obtained from ABAQUS

simulations showed excellent agreement with field measurements, validating the reliability of the ABAQUS model developed in this study. Consequently, the ABAQUS finite element software proves to be a valuable tool for further investigation of shear-lag effects in deck slabs.

IV. EFFECTIVE WIDTH ANALYSIS OF BRIDGE DECK

Taking working condition CC6 (the maximum double cantilever construction phase) as a case study, a more in-depth analysis of the shear lag effect on the main girder's concrete deck is performed.

A. Analysis of Shear Lag Effect in Standard Sections

To comprehensively evaluate the impact of edge steel box girders, transverse beams, and minor longitudinal beams on the shear-lag effect of the bridge deck, six cross-sections (designated as I-I to VI-VI) spaced at 2-meter intervals were selected within the standard main steel girder segment, as illustrated in Figure 9. Section VI-VI represents the intermediate section between two stay cables. Sections I-I, III-III, and V-V are directly connected to the transverse beams, whereas sections II-II, IV-IV, and VI-VI are situated at the midpoints between adjacent transverse beams. Specifically, the stress test section S1 aligns with section V-V in girder segment #1, section S2 corresponds to section III-III in girder segment #6, and section S3 matches section V-V in girder segment #16.

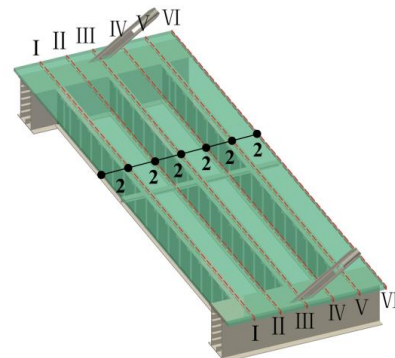
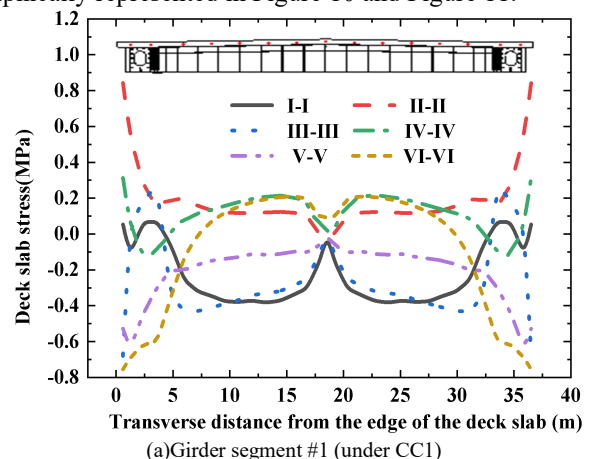
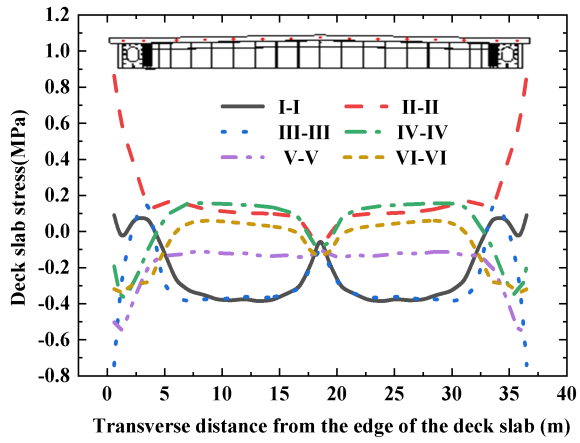


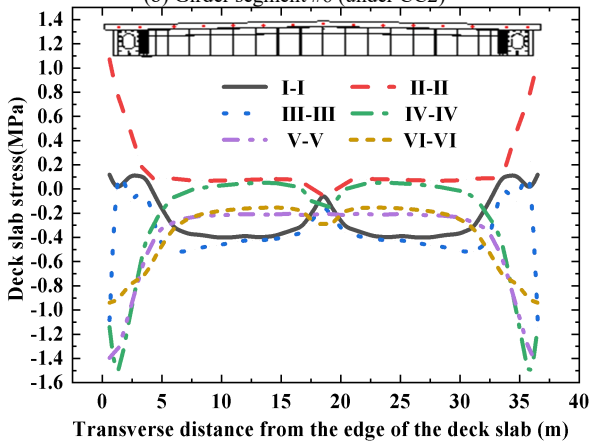
Fig. 9 Schematic diagram of six sections in the bridge transverse direction in the standard segment (unit: m)

Utilizing the ABAQUS finite element software, an analysis was conducted to determine the stresses across six deck slab cross-sections within girder segment #1 under loading condition CC1, segment #6 under CC2, and segment #16 under CC3, as well as segments #1, #6, and #16 under loading condition CC6. The results of this analysis are graphically represented in Figure 10 and Figure 11.



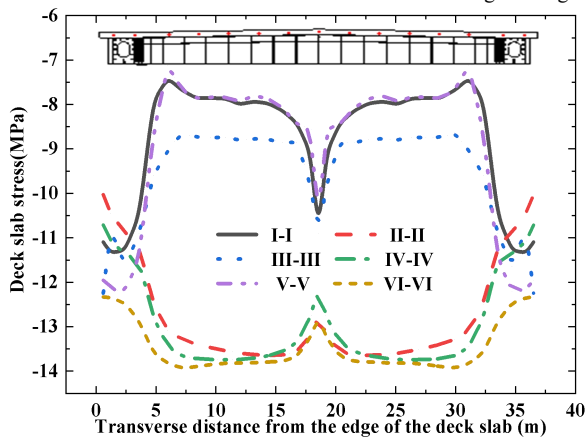


(a) Girder segment #1

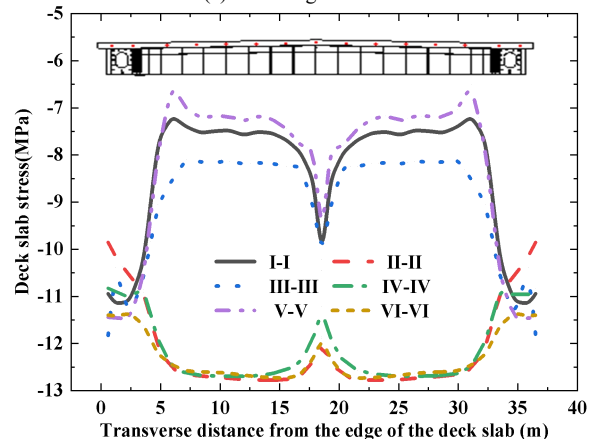


(b) Girder segment #6 (under CC2)

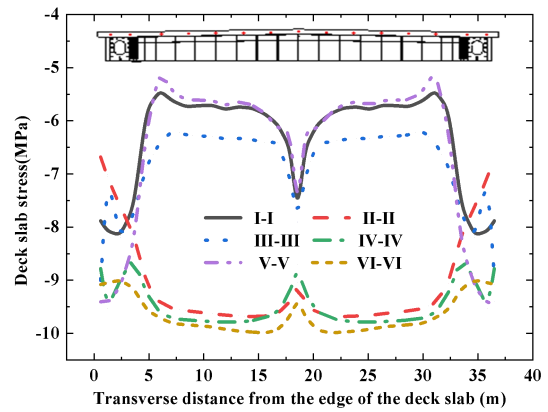
Fig. 10 Deck slab stress values at different cross-sections of girder segments



(c) Girder segment #16



(d) Girder segment #6 (under CC6)



(c) Girder segment #16

Fig. 11 Deck slab stress values at different cross-sections of girder segments (under CC6)

As illustrated in Figure 10 and Figure 11, the following observations can be made: 1) Following the tensioning of the stay cables, the shear-lag effect on the deck becomes pronounced, particularly at the junction of the anchor plate and the outer web of the side box girder, where the deck stress exhibits a significant abrupt change; 2) As construction progressed, the deck underwent a transition from a negative to a positive shear-lag effect. For example, the deck at the anchorage section (section III-III) of previously constructed girder segments shifted from a negative to a positive shear-lag effect, while the positive shear-lag effect in the deck slab along the mid-section between the stay cables (section VI-VI) transitioned to a negative shear-lag effect; 3) The presence of transverse beams and their shear connectors significantly influenced the shear-lag effect in the deck slab. For instance, during the maximum balanced cantilever construction phase, a distinct positive shear-lag effect was observed in the deck slabs of sections connected to the transverse beams (sections I-I, III-III, and V-V), whereas sections not connected to the transverse beams exhibited a noticeable negative shear-lag effect; 4) Finally, an abrupt stress change occurred in the deck slabs of all sections at the location of the small longitudinal beams, where the stress values approached the theoretical predictions of elementary beam theory. It indicates that the installation of small longitudinal beams can mitigate the shear-lag effect to some extent.

B. Coefficient of shear lag for bridge deck slabs

The magnitude of shear-lag can be characterized by a shear-lag coefficient, expressed as follows.

$$\lambda = \frac{\sigma_{\max}}{\bar{\sigma}} \quad (1)$$

where λ is shear lag coefficient, $\bar{\sigma}$ is the normal stress of the concrete slab calculated by elementary beam theory, σ_{\max} is the peak normal stress in the concrete slab. The shear-lag coefficient is defined as the ratio of the simulation results obtained from ABAQUS to those derived from MIDAS (based on elementary beam theory). Figure 12 presents the shear-lag coefficients for the cable anchorage section (Section III-III) and the mid-span section between stay cables (Section VI - VI) under CC6 loading condition, where X denotes the distance from the respective section to the bridge

pylon's center-line. The results demonstrate that during the maximum balanced cantilever construction stage, the anchorage section exhibits a pronounced positive shear-lag effect, while the mid-span section between stay cables shows a distinct negative shear-lag effect. Throughout the construction progression, the shear-lag coefficients in previously completed girder segments generally stabilized, with the exception of localized areas at the interface between the anchor plate and outer web, as well as near the small longitudinal beams.

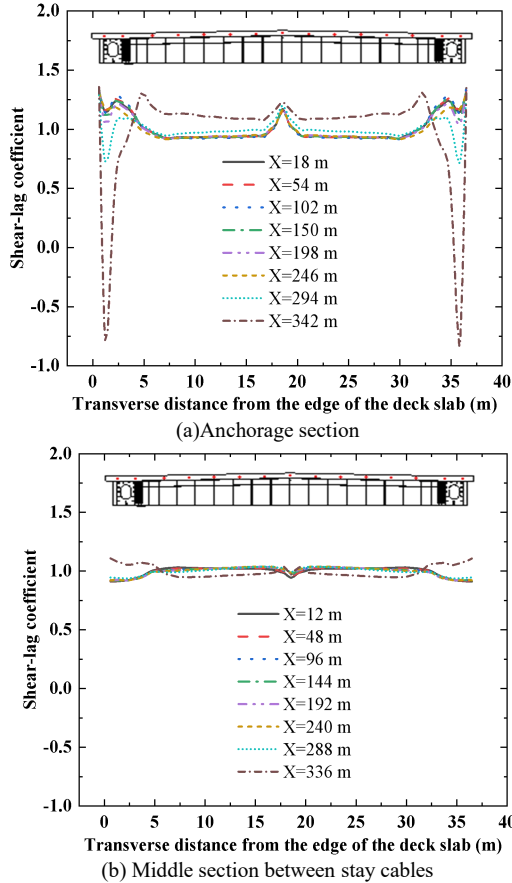


Fig. 12 Shear-lag coefficient of each cross-section deck (under CC6, X denotes the distance between the test section and the center-line of the pylon)

C. Effective Width of Bridge Deck

Extensive research and analytical studies have demonstrated that significant shear lag effects occur at both the anchorage sections and intermediate spans between stay cables during the construction of double-box composite girder cable-stayed bridges. Current design specifications lack explicit guidelines for determining the effective width of main girders in composite cable-stayed bridges. Furthermore,

the presence of anchored cables induces non-uniform distribution of effective width along the span direction. To address these issues, this study establishes finite element (FE) models of the Chibi Yangtze River Bridge, focusing on critical construction phases, to systematically investigate the longitudinal distribution characteristics of effective width.

The evaluation of the slab effective width in a given section requires the knowledge of the total resultant force (Q_i) that is applied in this section, as well as the maximum stress (σ_{max}) applied. Once the values of Q_i and σ_{max} are known from the FE results, the calculation of effective width (B_{eff}) is done through the following expression:

$$B_{eff} = \frac{Q_i}{\sigma_{max} \cdot t_c} \quad (2)$$

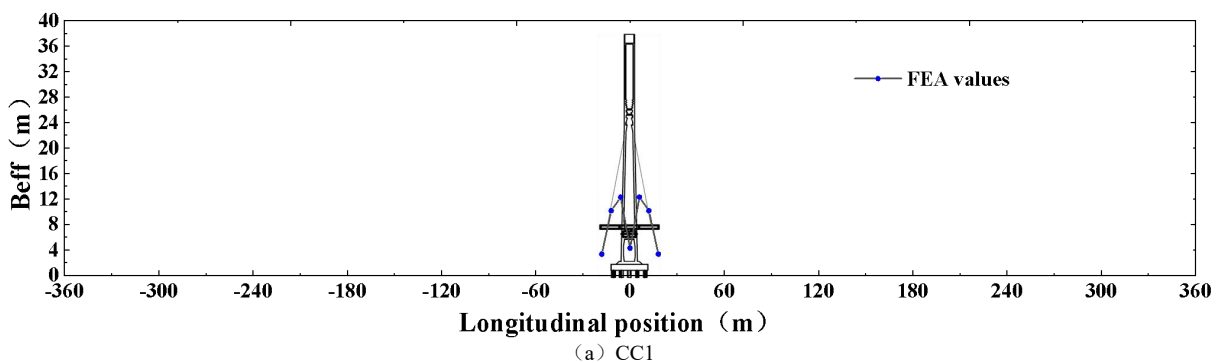
where Q_i is the longitudinal resultant force of the section; σ_{max} is the maximum normal stress of the section; t_c is the thickness of the concrete slab; B_{eff} is the effective width.

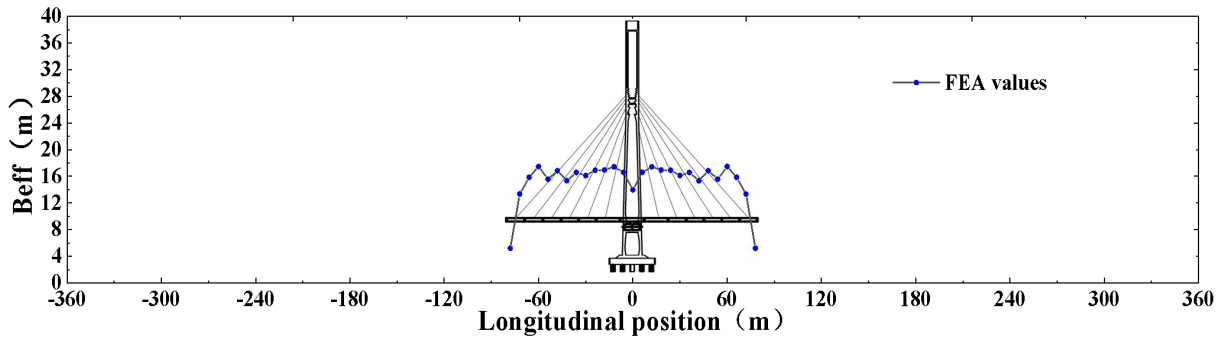
The calculated value of Q_i is done using an integration of tension along the width of the concrete slab. The use of finite elements transforms the applied stress in the section of the slab in a discrete system.

$$Q_i = \sum_{i=1}^n \sigma_i b_i t_i \quad (3)$$

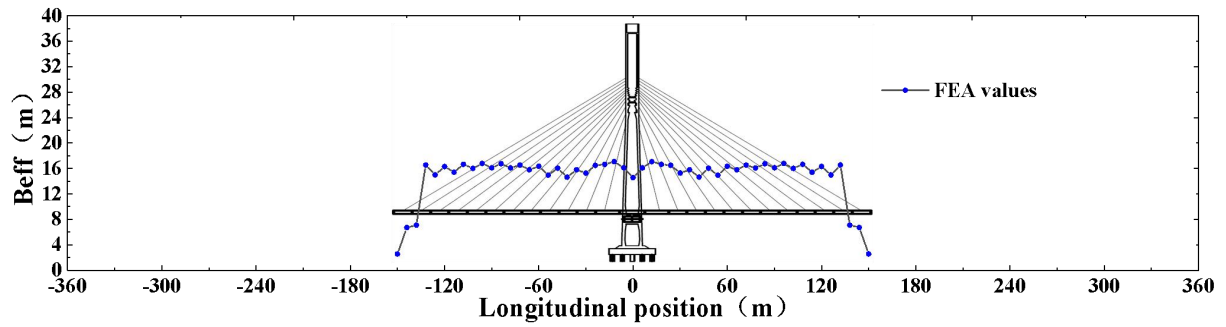
where σ_i is the normal stress of a certain element of the cross-section; b_i is the width of an element; t_i is the thickness of an element.

The variation of the effective width along the longitudinal direction under load cases CC1 to CC6 is illustrated in Figure 13. It can be seen from the figure that the calculated effective width of the bridge deck demonstrates significant variability across the span. Influenced by the axial forces exerted by the stay cables, the effective width of the bridge deck exhibits localized fluctuations along the bridge's longitudinal axis. Within these fluctuating regions, the effective width coefficient follows a distinct pattern: it is greatest at the cable anchorage sections, followed by the sections connected to the crossbeams, and smallest in the intermediate sections between two cables. Under the combined effects of axial forces and bending moments from the stay cables, the effective width of the concrete bridge deck at the auxiliary pier's top is notably reduced. Similarly, the effective width at the pylon locations and the mid-span of the main span is considerably smaller compared to other segments of the bridge. The smallest effective width is observed at the free end of the girder.

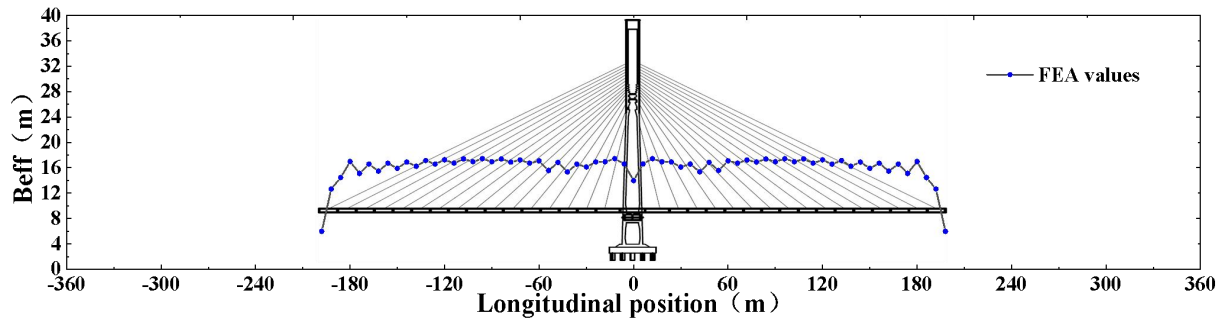




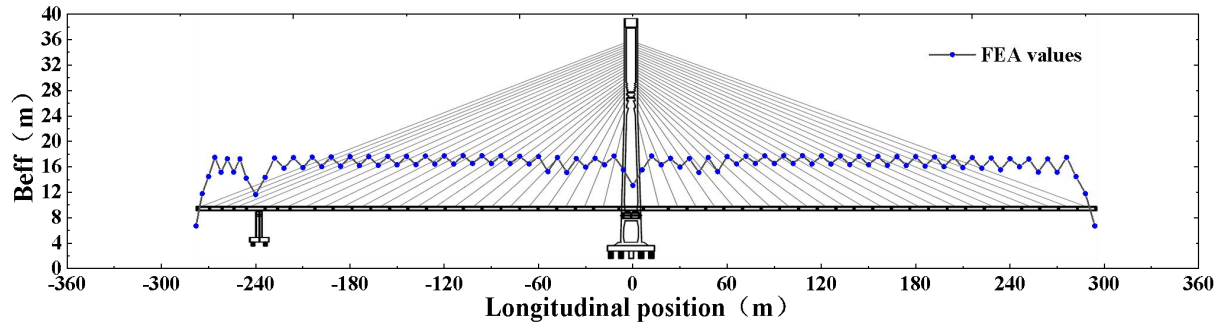
(b) CC2



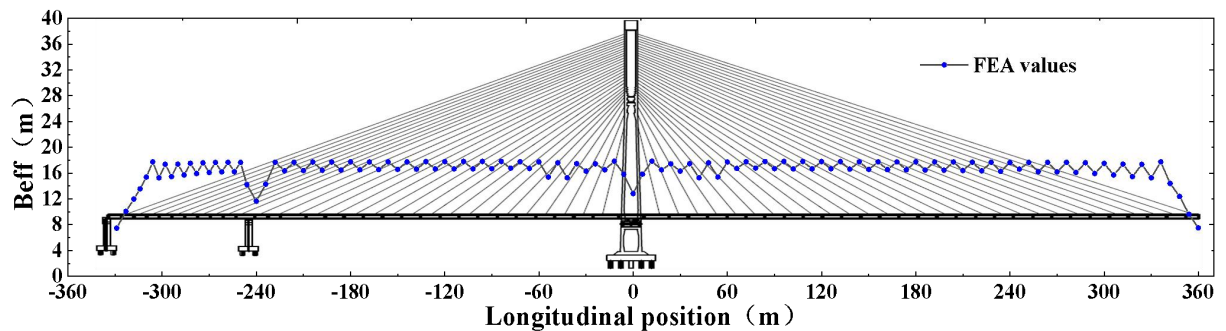
(c) CC3



(d) CC4



(e) CC5



(f) CC6

Fig. 13 Distribution of effective width of bridge deck along the longitudinal direction under different operating conditions

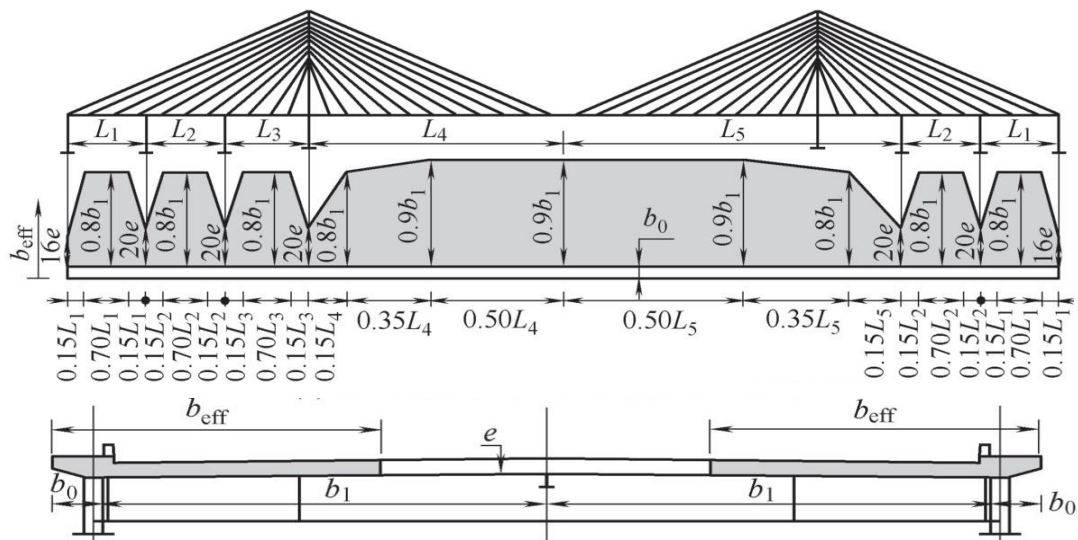


Fig. 14 Effective slab width for a composite cable-stayed deck [20]

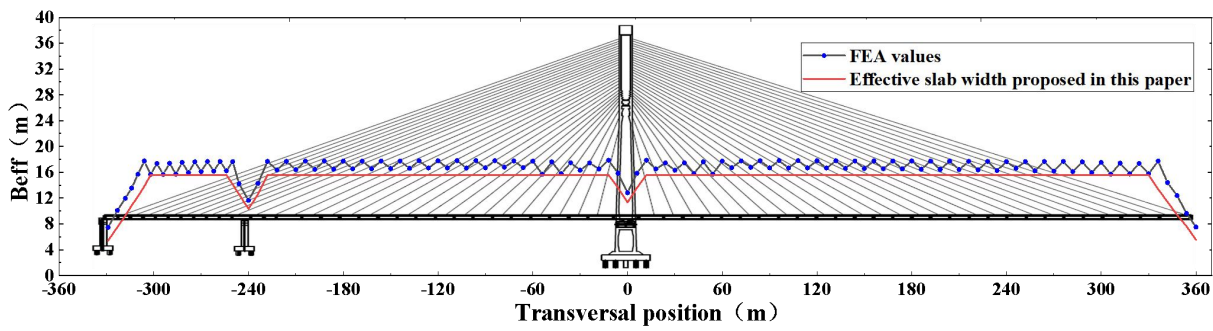


Fig. 15 Comparison of the effective width of the bridge deck proposed in this paper and the finite element calculation results

Byers [20] developed 18 sets of three-dimensional finite element (FE) models based on the structural parameters of an existing composite cable-stayed bridge in the United States to investigate the effective slab width in cable-stayed bridge design. In his study, he introduced a refined methodology for determining the effective distribution width specifically tailored for composite girder cable-stayed bridges. The research findings indicate that the effective width of the bridge deck in cable-stayed bridges is primarily dependent on three key parameters: the span length, deck plate thickness, and the actual width of the bridge deck, as illustrated in Figure 14.

The finite element analysis (FEA) results of the Chibi Yangtze River Highway Bridge (Figure 15, FEA values) reveal notable discrepancies between the longitudinal effective width distribution patterns observed in this study and those presented in Figure 14. Notably, the effective width values exhibit a significant reduction at the main span center in Figure 15, contrasting with the uniform distribution shown in Figure 14. Taking CC6 as a representative case, an envelope diagram of the longitudinal effective width distribution derived from finite element calculations is drawn (Figure 15, effective slab width proposed in this paper). The analysis indicates three key characteristics: (1) the effective width values exhibit localized amplitude oscillations along the longitudinal axis, (2) a progressive reduction in effective width is observed approaching the tower regions, and (3) at the auxiliary piers, the combined action of negative bending

moments and inclined cable axial forces creates a complex stress state characterized by simultaneous tension and compression in different portions of the main girder. The stress complexity leads to highly non-uniform stress distribution and consequently reduced effective width. Furthermore, the shear lag effect near the span center is particularly significant, with an effective width coefficient reaching as low as 0.41.

Based on the analysis of results presented in Figure 15, modifications have been incorporated into the rules initially proposed in Figure 14. Figure 16 illustrates a refined longitudinal distribution model for slab effective width, specifically developed for the structural analysis and design of composite cable-stayed bridges examined in this study. This enhanced model represents a significant improvement over Byers' original proposal, particularly through its incorporation of construction stage effects, thereby providing a more realistic representation of long-span composite cable-stayed bridge behavior. The proposed calculation methodology offers comprehensive consideration of critical structural zones where significant variations in effective width occur, including: (1) regions adjacent to main tower bearings, (2) areas near auxiliary piers, (3) girder end sections, and (4) the main span center. These variations result from the complex interaction between axial forces and bending moments in the stay cables. The developed methodology provides valuable reference data for the design and analysis of similar bridge structures.

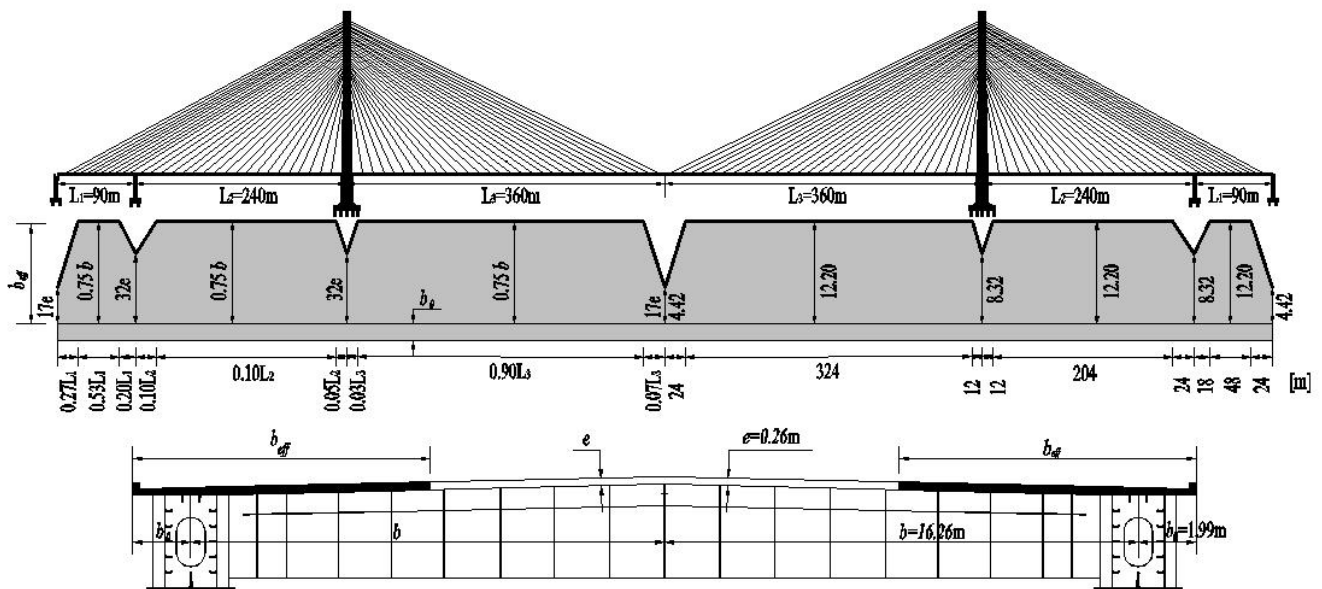


Fig. 16 Effective width of composite cable-stayed bridge deck

V. CONCLUSION

Drawing upon both field measurement data and finite element analysis results, the key findings of this study are summarized as follows:

(1)The transverse stress distribution in the concrete deck slab during the main girder's balanced cantilever assembly construction is characterized by non-uniformity, exhibiting stress concentrations confined to an effective width range adjacent to steel edge box girders, transverse beams, and small longitudinal beams, which manifests a marked shear lag phenomenon. A notable phenomenon of abrupt stress changes is observed in the deck slab at the junction of the anchor plate and the outer web of the side steel box girder. To ensure structural safety under load, the design can incorporate increased thickness of the flange plate and web or the addition of stiffeners. Furthermore, significant stress changes are also observed at the locations of the small longitudinal beams, with stress values closely aligning with those predicted by elementary beam theory. It suggests that the installation of small longitudinal beams mitigates the shear-lag effect to some extent. However, for conservative design calculations, the influence of small longitudinal beams can be disregarded.

(2)During the maximum double cantilever construction stage, a comparative analysis involving field-measured data, ABAQUS values, and elementary beam theory values indicates a maximum difference of 12.23% between ABAQUS values and field-measured data. The ABAQUS values exhibit consistent distribution patterns with field measured data in the bridge's transverse direction. This suggests the potential for further refined research using ABAQUS finite element software.

(3)As construction progresses, the deck slab stresses in girder segments exhibit significant variations primarily at the anchorage plate-outer web interface and small longitudinal beam locations. Stress distributions progressively homogenize in tower-adjacent segments, evidenced by stabilized shear lag coefficients. Notably, stress polarity

inversion occurs between cable-anchored sections (positive lag) and mid-span stay cable regions (negative lag).

(4) The axial forces exerted by the stay cables induces localized oscillations in the effective width values along the longitudinal direction. The effective width coefficient in these oscillating regions follows a pattern: maximum at the stay cable anchorage zones, followed by crossbeam connection sections, and minimum at the intermediate sections between adjacent stay cables. Under the combined influence of the axial forces and bending moments from the stay cables, the effective width at the auxiliary pier is relatively small. Similarly, the effective width near the main tower and at the mid-span of the main span is significantly reduced compared to other sections of the bridge, with the smallest effective width observed at the free end of the girder. Additionally, at the auxiliary piers, the main girder experiences partial tension and compression due to the negative bending moment and axial force from the inclined cable, leading to highly uneven stress distribution and a smaller effective width. The shear-lag effect near the mid-span is particularly pronounced, with an effective width coefficient of 0.41.

(5)This study proposes a longitudinal distribution model for slab effective width, specifically developed for the analysis and design of composite cable-stayed bridges. The proposed model effectively accounts for the substantial variations in deck effective width at critical locations, including regions adjacent to main tower bearings, auxiliary piers, girder ends, and the main span center. These variations result from the combined effects of axial forces and bending moments induced by stay cables. The developed model serves as a valuable reference for the design calculations of similar cable-stayed bridge structures, providing engineers with a reliable tool for addressing complex effective width distribution patterns.

REFERENCES

[1] H. G. Kwak , and J. W. Hwang, "Non-linear Finite Element Analysis of a Steel-concrete Composite Beam under Cyclic Loads Considering

- Interface Slip Effects,” *Engineering Letters*, vol.19, no.3, pp249-254, 2011
- [2] H Luo, et al. “Analysis of Shear Lag Effect of Steel-Concrete Composite Box Girders with Straight Steel Webs,” *IAENG International Journal of Applied Mathematics*, vol.54, no.3, pp507-517, 2024
- [3] R.S. Nicoletti, et al. “Numerical assessment of effective width in steel-concrete composite box girder bridges with partial interaction,” *Engineering Structures*, vol.239, pp112333, 2021
- [4] S.H. Yuan, et al. “Analysis of shear lag effect of extradosed cable-stayed bridges with corrugated steel webs during construction,” *Journal of Central South University(Science and Technology)*, vol.52, no.11, pp4055-4062, 2021 (in Chinese)
- [5] S.H. Jiang, H.T. Wu, and X.G. Liu, “Analysis of effective flange width in negative moment area of U-shaped steel concrete simply supported composite beams with external inversion,” *Sichuan Building Science*, vol.50, no.2, pp41-48+57, 2024 (in Chinese)
- [6] K.X. Chen, “Study on Effective Width of Composite Deck of Long-span Closed Steel-box Composite Girder,” *Urban Roads Bridges & Flood Control*, vol.2024, no.2, pp214-219+229+22, 2024 (in Chinese)
- [7] Y.L. Lin, “Study on Effective Width Coefficient of Composite Beam Deck of High Speed Railway Cable-stayed Bridge,” *Railway Engineering*, vol.63, no.11, pp62-68, 2023 (in Chinese)
- [8] Z.Y. Wen, et al. “Research on Effective Width of Composite Continuous Girder with Variable Stiffness,” *China Railway Science*, vol.43, no.4, pp1-8, 2022 (in Chinese)
- [9] X.H. Zhou, J Di, and G.L. Dai, “Study on segmental mode of girder of long-span prestressed concrete cable-stayed bridge,” *China Civil Engineering Journal*, vol.38, no.3, pp59-63, 2005 (in Chinese)
- [10] J.G. Nie, F.X. Li, and J.S. Fan, “Study on effective width of concrete deck in composite cable-stayed bridge,” *Journal of Harbin Institute of Technology*, vol.39, no.2, pp7193-724, 2007 (in Chinese)
- [11] X.L. Zhai, et al. “Effective width coefficient for composite cable-stayed bridge and its practical calculation method,” *Journal of Chang'an University (Natural Science Edition)*, vol.33, no.01, pp51-58, 2013 (in Chinese)
- [12] F.G. Gian, et al. “Calculating shear lag in steel-concrete composite beams under combined compression and bending,” *Engineering Structures*, vol.322, pp119101, 2024
- [13] W.T. Zhang, et al. “A theoretical model for investigating shear lag in composite cable-stayed bridges,” *Frontiers of Structural and Civil Engineering*, vol.17, no.12, pp1907-1923, 2023
- [14] Z.Y Wen, et al. “Experiment and Modelling on Effective Width of Single and Twin I-beam Composite Girders,” *KSCE Journal of Civil Engineering*, vol.27, no.6, pp2559-2569, 2023
- [15] Y.Q. Huang, et al. “Prediction for Effective Flange Width of Steel-Concrete Composite Beam with TALHGs,” *Arabian Journal for Science and Engineering*, vol.47, pp5199-5218, 2022
- [16] R.N. Silva, et al. “Numerical assessment of effective width in steel-concrete composite box girder bridges,” *Advances in Structural Engineering*, vol.24, no.5, pp977-994, 2021
- [17] Y.J. Zhu, et al. “Prediction model for load effective distribution width of slab in composite box girders using gene expression programming,” *Engineering Structures*, vol.255, pp113930, 2022
- [18] M Lasheen, A Shaat, and A Khalil. “Numerical evaluation for the effective slab width of steel-concrete composite beams,” *Journal of Constructional Steel Research*, vol.148, pp124-137, 2018
- [19] L Galuppi and GRoyer-Carfagni. “Effective Width of the Slab in Composite Beams with Nonlinear Shear Connection,” *Journal of Engineering Mechanics*, vol.142, no.45, pp04016001-04016001, 2016
- [20] D. Byers, “Evaluation of the Effective Slab Width for Composite Cable-Stayed Bridge Design,” Ph.D.Thesis. University of Kansas,1999



Jianqiang Feng was born in December 1998 and received his B.E. Degree from Hunan Institute of Science and Technology, Yueyang, China, in 2021. His research interest is mainly on the shear lag effect of steel-concrete composite girders. Jianqiang Feng is a postgraduate student in Hunan Institute of Science and Technology. He has authored or co-authored 2 journal papers.



Dr. Qincong She was born in July 1987 and received his Ph.D. Degree from Changsha University of Science and Technology, Changsha, China, in 2024. His research interests are mainly on bridge construction monitoring and steel-concrete composite structure. Qincong She has worked as a lecturer in Hunan Institute of Science and Technology. He has authored or co-authored 10 journal papers to date.



Dr. Bin Li was born in December 1981 and received his Ph.D. Degree from Changsha University of Science and Technology, Changsha, China, in 2017. He is an associate professor in College of Civil Engineering and Architecture, Hunan Institute of Science and Technology, Yueyang, China. His research interests cover bridge engineering and engineering mechanics. He has published more than 30 technical papers.



Dr. Yongqing Zeng was born in February 1991 and received his M.S.Degree from Anhui University of Science and Technology, Huainan, China, in 2016, and received the Ph.D. degree from Institute of Rock and Soil Mechanics, Chinese Academy of Sciences, Wuhan, China, in 2019. His research interests are mainly on geotechnical engineering. Yongqing Zeng has worked as an associate professor in Hunan Institute of Science and Technology. He authored or co-authored 25 journal papers and 5 international conference papers to date.



Dr. Hua Luo was born in September 1985 and received her Ph.D. Degree from Beijing Jiaotong University, Beijing, China, in 2015. She is an associate professor in College of Civil Engineering and Architecture, Hunan Institute of Science and Technology, Yueyang, China. Her research interests cover bridge engineering and composite structure. She has published more than 20 technical papers.